48th AIAA/ASME/ASCE/AHS/ASC Structures, Structural Dynamics, and Materials Conference
23 - 26 April 2007, Honolulu, Hawaii

AIAA 2007-1934

Solution-Verified Reliability Analysis and Design of Compliant Micro-Electro-Mechanical Systems

M. S. Eldred,* B. M. Adams,† K. D. Copps,‡ B. Carnes,§
P. K. Notz,¶ M. M. Hopkins,‖ and J. W. Wittwer,**
Sandia National Laboratories,††Albuquerque, NM 87185

An important component of verification and validation of computational models is solution verification, which focuses on the convergence of the desired solution quantities as one refines the spatial and temporal discretizations and iterative controls. Uncertainty analyses often treat solution verification as a separate issue, hopefully through the use of *a priori* grid convergence studies and selection of models with acceptable discretization errors. In this paper, a tighter connection between solution verification and uncertainty quantification is investigated. In particular, error estimation techniques, using global norm and quantity of interest error estimators, are applied to the nonlinear structural analysis of microelectromechanical systems (MEMS). Two primary approaches for uncertainty quantification are then developed: an error-corrected approach, in which simulation results are directly corrected for discretization errors, and an error-controlled approach, in which estimators are used to drive adaptive h-refinement of mesh discretizations. The former requires quantity of interest error estimates that are quantitatively accurate, whereas the latter can employ any estimator that is qualitatively accurate. Combinations of these error-corrected and error-controlled approaches are also explored. Each of these techniques treats solution verification and uncertainty analysis as a coupled problem, recognizing that the simulation errors may be influenced by, for example, conditions present in the tails of input probability distributions. The most effective and affordable of these approaches are carried forward in probabilistic design studies for robust and reliable operation of a bistable MEMS device. Computational results show that on-line and parameter-adaptive solution verification can lead to uncertainty quantification and design under uncertainty studies that are more accurate, efficient, reliable, and convenient.

I. Introduction

Pre-fabrication design optimization of microelectromechanical systems (MEMS) is an important emerging application of uncertainty quantification and reliability-based design optimization. Typically crafted of silicon, polymers, metals, or a combination thereof, MEMS serve as micro-scale sensors, actuators, switches, and machines with applications including robotics, biology and medicine, automobiles, RF electronics, and optical displays.[1] Design optimization of these devices is crucial due to high cost and long fabrication timelines. Uncertainty in the micromachining and etching processes used to manufacture MEMS can lead to large uncertainty in the behavior of the finished products, resulting in low part yield and poor durability. Reliability-based design optimization (RBDO), coupled with computational mechanics models of MEMS,

*Principal Member of Technical Staff, Optimization and Uncertainty Estimation Department, MS-1318, Associate Fellow AIAA.
†Limited Term Member of Technical Staff, Optimization and Uncertainty Estimation Department, MS-1318, Member AIAA.
‡Senior Member of Technical Staff, Advanced Computational Mechanics Architectures Department, MS-0382.
§Senior Member of Technical Staff, Advanced Computational Mechanics Architectures Department, MS-0382.
¶Senior Member of Technical Staff, Multiphase and Nanoscale Transport Processes Department, MS-0836.
‖Senior Member of Technical Staff, Multiphase and Nanoscale Transport Processes Department, MS-0836.
**Senior Member of Technical Staff, MEMS Devices and Reliability Physics, MS-1310.
††Sandia is a multiprogram laboratory operated by Sandia Corporation, a Lockheed Martin Company, for the United States Department of Energy's National Nuclear Security Administration under Contract DE-AC04-94AL85000.

offers a means to quantify this uncertainty and determine a priori the most reliable and robust designs that meet performance criteria.[2]

Uncertainty quantification (UQ) is the process of determining the effect of input uncertainties on response metrics of interest. These input uncertainties may be characterized as either aleatory uncertainties, which are irreducible variabilities inherent in nature, or epistemic uncertainties, which are reducible uncertainties resulting from a lack of knowledge. Since sufficient data is generally available for aleatory uncertainties, probabilistic methods are commonly used for computing response distribution statistics based on input probability distribution specifications. Conversely, for epistemic uncertainties, data is generally sparse, making the use of probability theory questionable and leading to nonprobabilistic methods based on interval specifications.

For the MEMS problems of interest, data on manufacturing variabilities is generally available and probabilistic methods may be used. The technique selected for performing UQ in this study is reliability analysis, which quantifies the effect of aleatory input uncertainties defined by probability distributions. This class of UQ methods is often more efficient at computing statistics in the tails of the response distributions (events with low probability) than sampling-based approaches because the number of samples required to resolve a low probability can be prohibitive. Thus, these methods, as their name implies, are often used in a reliability context for assessing the probability of failure of a system when confronted with an uncertain environment.

A reliability analysis that captures the effect of random variables on response metrics for an inaccurate, inappropriate, or unconverged model is of limited utility. For this reason, it is prudent to pursue verification and validation activities for the computational model of interest. One portion of this is the area of solution verification, which focuses on the convergence of the desired solution quantities as one refines the spatial and temporal discretizations and iterative controls. When these convergence analyses are performed off-line, they may result in a relatively expensive model that has been verified for a single set of nominal design/uncertain parameters. With the advent of finite element error estimation techniques, techniques for on-line and parameter-adaptive solution verification become possible and hold potential for improving overall accuracy and efficiency.

A number of different conceptual formulations are possible for incorporating errors and uncertainties. If the discretization errors are not driven toward zero through the use of mesh refinement (in an error-controlled approach), then they can be included within the uncertainty analysis (in an error-corrected approach) using one of the following conceptual models:

1. given error estimates for the response quantities of interest, model the discretization error as a deterministic quantity that can correct results for a particular mesh discretization. The results generated from the uncertainty analysis are then projected towards the fully converged results, but uncertainties in the accuracy of the error estimates are not modeled.

2. given error estimates for the response quantities of interest, model the true discretization error as being uncertain since the estimate will not in general be exact. In particular, model the discretization error as a random variable and incorporate it as an additional uncertainty within the probabilistic analysis.

3. given error bounds for the response quantities of interest, model the true discretization error as an additional uncertainty within the UQ analysis. Given no additional data on the error distribution within the bounds, modeling the error as an epistemic uncertainty using an interval distribution would be appropriate.

Put another way, one can attempt to eliminate the errors (through uniform or adaptive mesh refinement), account for the errors deterministically (approach 1), or account for the errors probabilistically (approaches 2 and 3). In this study, we employ approach 1, and do not model the discretization error as a random quantity. In addition, error bounds are more challenging to obtain and are outside the scope of this paper. Approaches 2 and 3 are directions for future research.

Our test problem for solution-verified reliability analysis comes from the structural mechanics simulation of a bistable MEMS switch. The geometric nonlinearity and large displacements of the problem motivate a fully nonlinear finite strain 2D elasticity model for the bistable switch. In order to compute an estimate of the error in the force at each displacement step resulting from the mesh discretization, an *a posteriori* error estimate was derived for this quantity of interest. This "goal-oriented" estimator is defined by integrating the finite element residual weighted by the error in an associated global linearized adjoint problem. Local

element contributions to the global error estimate can then be used to drive adaptive mesh refinement. In this case, the mesh is adapted to minimize the error in the force, which is known as goal-oriented adaptivity.

Sections II, III, and IV describe the reliability analysis, error estimation, and reliability-based design optimization algorithms, respectively. Section V describes their application to a microelectromechanical compliant bistable mechanism, Section VI presents computational results, and Section VII provides concluding remarks.

II. Reliability Method Formulations

Reliability methods are probabilistic algorithms for quantifying the effect of input uncertainties on response metrics of interest. In particular, they perform uncertainty quantification (UQ) by computing approximate response distribution statistics based on specified probability distributions for input random variables. These response statistics include mean, standard deviation, and cumulative or complementary cumulative distribution function (CDF/CCDF) response level and probability level pairings.

Refs. 3 and 4 describe a variety of first-order and second-order algorithms for reliability analysis, including Mean Value (MV, also known as MVFOSM), Advanced Mean Value (AMV), iterated Advanced Mean Value (AMV+), second-order iterated Advanced Mean Value (AMV^2+), two-point adaptive nonlinearity approximation (TANA), and the first-order and second-order reliability methods (FORM and SORM). MV is the simplest, least-expensive reliability method because it estimates the response means, response standard deviations, and all CDF/CCDF response-probability-reliability levels from a single evaluation of response functions and their gradients at the uncertain variable means. This approximation can have acceptable accuracy when the response functions are nearly linear and their distributions are approximately Gaussian, but can have poor accuracy in other situations. All other reliability methods solve a nonlinear equality-constrained optimization problem to compute a most probable point (MPP) and then integrate about this point to compute probabilities. The MPP search is performed in uncorrelated standard normal space ("u-space") since it simplifies the probability integration. The transformation from correlated non-normal distributions (x-space) to uncorrelated standard normal distributions (u-space) is denoted as $\mathbf{u} = T(\mathbf{x})$ with the reverse transformation denoted as $\mathbf{x} = T^{-1}(\mathbf{u})$. These transformations are nonlinear in general, and possible approaches include the Rosenblatt,[5] Nataf,[6] and Box-Cox[7] transformations. The nonlinear transformations may also be linearized, and common approaches for this include the Rackwitz-Fiessler[8] two-parameter equivalent normal and the Chen-Lind[9] and Wu-Wirsching[10] three-parameter equivalent normals. The results in this paper employ the Nataf nonlinear transformation which occurs in the following two steps. To transform between the original correlated x-space variables and correlated standard normals ("z-space"), the CDF matching condition is used:

$$\Phi(z_i) = F(x_i) \tag{1}$$

where $\Phi()$ is the standard normal cumulative distribution function and $F()$ is the cumulative distribution function of the original probability distribution. Then, to transform between correlated z-space variables and uncorrelated u-space variables, the Cholesky factor $\mathbf{L}$ of a modified correlation matrix is used:

$$\mathbf{z} = \mathbf{L}\mathbf{u} \tag{2}$$

where the original correlation matrix for non-normals in x-space has been modified to represent the corresponding correlation in z-space.

The forward reliability analysis algorithm of computing CDF/CCDF probability p or reliability β levels for specified response levels $\bar{z}$ is called the reliability index approach (RIA), and the inverse reliability analysis algorithm of computing response levels z for specified CDF/CCDF probability $\bar{p}$ or reliability levels $\bar{\beta}$ is called the performance measure approach (PMA).[11] The differences between the RIA and PMA formulations appear in the objective function and equality constraint formulations used in the MPP searches. For RIA, the MPP search for achieving the specified response level $\bar{z}$ is formulated as

$$\begin{aligned} \text{minimize} \quad & \mathbf{u}^T\mathbf{u} \\ \text{subject to} \quad & G(\mathbf{u}) = \bar{z} \end{aligned} \tag{3}$$

and for PMA, the MPP search for achieving the specified reliability/probability level $\bar{\beta}, \bar{p}$ is formulated as

$$\begin{aligned} \text{minimize (or maximize)} \quad & G(\mathbf{u}) \\ \text{subject to} \quad & \mathbf{u}^T\mathbf{u} = \bar{\beta}^2 \end{aligned} \tag{4}$$

where $\mathbf{u}$ is a vector centered at the origin in u-space, $g(\mathbf{x})$ is the limit state function (the response function for which probability-response level pairs are needed), and $g(\mathbf{x}) \equiv G(\mathbf{u})$ by definition. In the RIA case, the optimal MPP solution $\mathbf{u}^*$ defines the reliability index from $\beta = \pm\|\mathbf{u}^*\|_2$, which in turn defines the CDF/CCDF probabilities based on first-order integration (i.e., $p = \Phi(-\beta)$), second-order integration (e.g., Breitung, Hohenbichler-Rackwitz, or Hong corrections which use principal curvatures κ_i of the limit state function to better inform the integration), or (adaptive) importance sampling. In the PMA case, the limit state at the MPP ($G(\mathbf{u}^*)$) defines the desired response level result. Refer to Refs. 3 and 4 for information on sign conventions and other details.

There are a variety of algorithmic variations that can be explored within RIA/PMA reliability analysis including limit state approximations, probability integrations, warm starting approaches, Hessian approximations, and optimization algorithm selections.[3,4] The results in this paper come from optimizing the AMV^2+ approximation,[4] where a second-order Taylor series model of the limit state is used and updated as the optimization progresses with rank one updates to the Hessian and new expansions about each candidate MPP. When the desired statistics include probabilities, they are calculated by integrating around the most probable point in u-space using either first order or second-order integration methods. All of these reliability analysis capabilities are implemented in DAKOTA, an open-source software toolkit for design optimization, uncertainty quantification, parameter estimation, and sensitivity analysis.[12]

III. Error Estimation

We now describe the nonlinear elasticity problem that we will solve for the force response of the MEMS device. In addition, we outline the a posteriori error estimators that we use to compute the error in the force.

Suppose that we wish to solve the following nonlinear elasticity problem in a domain Ω: find the stress tensor field σ satisfying

$$-\nabla \cdot \sigma = f, \quad x \in \Omega. \tag{5}$$

In general σ is a nonlinear function of the displacment vector field u. Ω is the deformed reference frame, which is the image of the undeformed reference frame Ω_X under the mapping

$$x \equiv X + u \tag{6}$$

for any $X \in \Omega_X$.

The stress is a nonlinear function of the displacement gradients. In order to derive this expression, we first introduce the deformation gradient, which is the derivative of the mapping in (6)

$$F \equiv (\nabla_X x)^t = (\nabla_X X)^t + (\nabla_X u)^t = I + (\nabla_X u)^t. \tag{7}$$

The stress $\sigma = \sigma(\nabla u)$ is then given by the neo-Hookean constitutive model

$$\sigma \equiv \frac{\mu}{J}\left(F \cdot F^t - I\right) + \frac{\lambda \ln J}{J} I, \tag{8}$$

where $J \equiv \det F$ and λ and μ are the Lamé coefficients. For infinitessimal gradients $\nabla_X u$, the neo-Hookean model will reduce to the form of Hooke's law for linearized elasticity

$$\sigma \equiv 2\,\mu\,\varepsilon + \lambda\,(\operatorname{tr}\varepsilon)\,I, \quad \varepsilon \equiv \frac{1}{2}(\nabla_X u^t + (\nabla_X u)^t).$$

The nonlinearities in this problem arise from two main sources. First, the neo-Hookean model is a highly nonlinear function of the deformation gradient. Second, both the domain and the derivatives are functions of the displacement field.

In order to derive a weak variational formulation, we begin by multiplying (5) by a test function v and integrating by parts over Ω to obtain

$$\int_\Omega \sigma : \nabla v \, dx - \int_{\partial\Omega} \sigma \cdot n \, v \, ds = \int_\Omega f \, v \, dx. \tag{9}$$

We assign Dirichlet boundary conditions to part of the domain Γ_D

$$u = u_D, \tag{10}$$

and Neumann boundary conditions to the remainder Γ_N

$$\sigma \cdot n = g_N. \tag{11}$$

Substituting these into (9), we obtain the variational problem for u satisfying

$$\int_\Omega \sigma : \nabla v \, dx = \int_\Omega f \, v \, dx + \int_{\Gamma_N} g_N \, v \, ds, \tag{12}$$

for all test functions v that vanish on Γ_D. By choosing a finite dimensional space V_h, we can define a finite element approximation as the solution to th problem: find $u_h \in u_D + V_h$:

$$\int_\Omega \sigma_h : \nabla v_h \, dx = \int_\Omega f \, v_h \, dx + \int_{\Gamma_N} g_N \, v_h \, ds, \quad \forall v_h \in V_h, \tag{13}$$

where $\sigma_h = \sigma(\nabla u_h)$ is the discrete stress.

Suppose that we are interested in estimating the error in the i–th component of the surface traction over some segment $\Gamma_0 \subset \Gamma_D$

$$j(u) \equiv j_{i,\Gamma_0}(u) \equiv \int_{\Gamma_0} e_i \cdot \sigma(u) \cdot n \, ds. \tag{14}$$

In practice a more accurate postprocessed surface force is given by

$$j_h(u) \equiv \int_{\Gamma_0} \sigma(u) : \nabla \psi_h \, dx - \int_\Omega f \, \psi_h \, dx + \int_{\Gamma_N} g_N \, \psi_h \, ds. \tag{15}$$

Here the function ψ_h is defined as the finite element function which is one for nodes of component i on Γ_0 and zero for all other nodes.

Let z be the solution to the following linearized *adjoint* problem: find z such that

$$z = \begin{cases} e_i, & s \in \Gamma_0, \\ 0, & s \in \Gamma_D / \Gamma_0, \end{cases} \tag{16}$$

and

$$\int_\Omega (\sigma'(u_h) z) : \nabla \phi \, dx = 0, \quad v \in V. \tag{17}$$

Using this adjoint problem, we can derive the error estimate for the error $E \equiv j_h(u) - j_h(u_h)$ as

$$E = \int_\Omega \sigma(u_h) : \nabla (z - v_h) \, dx - \int_\Omega f \, (z - v_h) \, dx - \int_{\Gamma_N} g_N \, (z - v_h) \, ds + R, \quad \forall v_h \in V_h, \tag{18}$$

where R is a higher order remainder.

A practical error estimate based on (18) can be derived using an approximate dual solution. Let z_h be the finite element approximation to the adjoint solution z. Since the terms in 18 containing the data f and g_N are formally higher order, we can neglect them in a practical error estimate. Finally, we can use $v_h = z_h$, and approximate the exact gradients of z using a gradient recovery operator $R(\nabla z_h)$ based on z_h. The practical error estimator is then given by:

$$\eta^Q \equiv \int_\Omega \sigma(u_h) : (R(\nabla z_h) - \nabla z_h) \, dx. \tag{19}$$

The factors influencing the accuracy of the error indicator include the linearization error, the neglection of the higher order terms, the gradient recovery approximation, and error from numerical quadrature.

IV. Reliability-Based Design Optimization

Capabilities to assess reliability and estimate errors have thus far been discussed. The next step is to embed these procedures within the design optimization context, and we will employ reliability-based design optimization (RBDO) algorithms to perform solution-verified design under uncertainty. RBDO approaches

may be broadly characterized as bi-level (in which the reliability analysis is nested within the optimization[13]), sequential (in which iteration occurs between optimization and reliability analysis[14,15]), or unilevel (in which the design and reliability searches are combined into a single optimization[16]). The reliability analysis capabilities described in Section II provide a rich foundation for exploring a variety of RBDO formulations. Ref. 3 investigated bi-level, fully-analytic bi-level, and first-order sequential RBDO approaches employing underlying first-order reliability assessments. Ref. 4 investigated fully-analytic bi-level and second-order sequential RBDO approaches employing underlying second-order reliability assessments. The studies in this paper employ semi-analytic bi-level RBDO, where the semi-analytic nature arises from the combination of analytic probabilistic sensitivities with numerical simulation response sensitivities.

The bi-level RBDO approach performs a full reliability analysis for every optimization function evaluation. This involves a nesting of two distinct levels of optimization within each other, one at the design level and one at the MPP search level. Since an RBDO problem will typically specify both the $\bar{z}$ level and the $\bar{p}/\bar{\beta}$ level, one can use either the RIA or the PMA formulation for the UQ portion and then constrain the result in the design optimization portion. In particular, RIA reliability analysis maps $\bar{z}$ to p/β, so RIA RBDO constrains p/β:

$$\begin{aligned} \text{minimize} \quad & f \\ \text{subject to} \quad & \beta \geq \bar{\beta} \\ \text{or} \quad & p \leq \bar{p} \end{aligned} \tag{20}$$

And PMA reliability analysis maps $\bar{p}/\bar{\beta}$ to z, so PMA RBDO constrains z:

$$\begin{aligned} \text{minimize} \quad & f \\ \text{subject to} \quad & z \geq \bar{z} \end{aligned} \tag{21}$$

where $z \geq \bar{z}$ is used as the RBDO constraint for a cumulative failure probability (failure defined as $z \leq \bar{z}$) but $z \leq \bar{z}$ would be used as the RBDO constraint for a complementary cumulative failure probability (failure defined as $z \geq \bar{z}$).

An important performance enhancement for bi-level methods is the use of sensitivity analysis to analytically compute the design gradients of probability, reliability, and response levels. When design variables are separate from the uncertain variables (i.e., they are not distribution parameters), then the following first-order expressions may be used:[13,17,18]

$$\nabla_{\mathbf{d}} z = \nabla_{\mathbf{d}} g \tag{22}$$

$$\nabla_{\mathbf{d}} \beta_{cdf} = \frac{1}{\| \nabla_{\mathbf{u}} G \|} \nabla_{\mathbf{d}} g \tag{23}$$

$$\nabla_{\mathbf{d}} p_{cdf} = -\phi(-\beta_{cdf}) \nabla_{\mathbf{d}} \beta_{cdf} \tag{24}$$

In the case of second-order integrations, Eq. 24 must be expanded to include the curvature correction.[4] To capture second-order probability estimates within an RIA RBDO formulation using well-behaved β constraints, a generalized reliability index can be introduced where

$$\beta^*_{cdf} = -\Phi^{-1}(p_{cdf}) \tag{25}$$

for second-order p_{cdf}. This reliability index is no longer equivalent to the magnitude of $\mathbf{u}$, but rather is a convenience metric for capturing the effect of more accurate probability estimates. The corresponding generalized reliability index sensitivity is presented in Ref. 4. Even when $\nabla_{\mathbf{d}} g$ is estimated numerically, these probabilistic sensitivity equations can be used to avoid numerical differencing across full reliability analyses. This semi-analytic approach is the one adopted for the MEMS application explored in this paper.

When the design variables are distribution parameters of the uncertain variables, $\nabla_{\mathbf{d}} g$ is expanded with the chain rule and Eqs. 22 and 23 become

$$\nabla_{\mathbf{d}} z = \nabla_{\mathbf{d}} \mathbf{x} \nabla_{\mathbf{x}} g \tag{26}$$

$$\nabla_{\mathbf{d}} \beta_{cdf} = \frac{1}{\| \nabla_{\mathbf{u}} G \|} \nabla_{\mathbf{d}} \mathbf{x} \nabla_{\mathbf{x}} g \tag{27}$$

where the design Jacobian of the transformation ($\nabla_{\mathbf{d}} \mathbf{x}$) may be obtained analytically for uncorrelated $\mathbf{x}$ or semi-analytically for correlated $\mathbf{x}$ ($\nabla_{\mathbf{d}} \mathbf{L}$ is evaluated numerically) by differentiating Eqs. 1 and 2 with respect to the distribution parameters. All other equations remain the same as before. For this design variable case, all required information for the sensitivities is available from the MPP search.

V. Simulation of MEMS Bistable Mechanisms

MEMS bistable mechanisms toggle between two stable positions, making them useful as micro switches, relays, and nonvolatile memory. In particular, the focus here is on shape optimization of compliant bistable mechanisms, where instead of mechanical joints, material elasticity and geometry enable the bistability of the mechanism.[19–21] Figure 1(a) contains an electron micrograph of a MEMS compliant bistable mechanism in its second stable position. The first stable position is the as-fabricated position. One achieves transfer between stable states by applying force to the center shuttle via a thermal actuator, electrostatic actuator, or other means to move the shuttle past an unstable equilibrium.

Bistable switch actuation characteristics depend on the relationship between actuation force and shuttle displacement for the manufactured switch. Figure 1(b) contains a schematic of a typical force–displacement curve for a bistable mechanism. The switch characterized by this curve has three equilibria: E_1 and E_3 are stable equilibria whereas E_2 is an unstable equilibrium (arrows indicate stability). A device with such a force–displacement curve could be used as a switch or actuator by setting the shuttle to position E_3 as shown in Figure 1(a) (requiring large actuator force F_{max}) and then actuating by applying the comparably small force F_{min} in the opposite direction to transfer back through E_2 toward the equilibrium E_1. One could utilize this force profile to complete a circuit by placing a switch contact near the displaced position corresponding to maximum (closure) force as illustrated. Repeated actuation of the switch relies on being able to reset it with actuation force F_{max}.

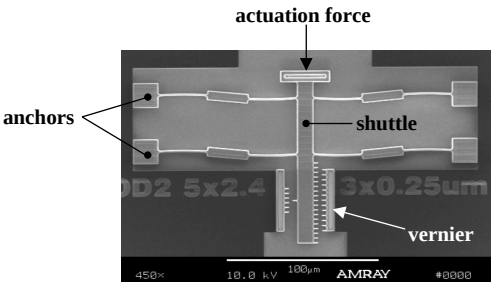

(a) Scanning electron micrograph of a MEMS bistable mechanism in its second stable position. The attached vernier provides position measurements.[22]

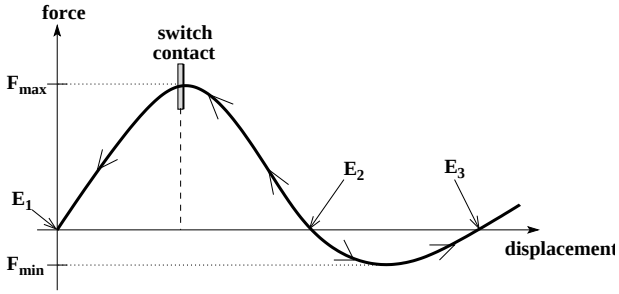

(b) Schematic of force–displacement curve for bistable MEMS mechanism. The arrows indicate stability of equilibria E_1 and E_3 and instability of E_2.

Figure 1. Bi-stable MEMS mechanism.

The device design considered in this paper is similar to that in the electron micrograph in Figure 1(a), for which design optimization has been previously considered,[21] as has robust design under uncertainty with mean value methods.[23] The primary structural difference in the present design is the tapering of the legs, shown schematically in Figure 2(a). Figure 2(b) shows a scale drawing of one tapered beam leg (one quarter of the full switch system). A single leg of the device is approximately 100 μm wide and 5–10 μm tall. This topology is a cross between the fully compliant bistable mechanism reported in Ref. 21 and the thickness-modulated curved beam in Ref. 24. As described in the optimization problem below, this tapered geometry offers many degrees of freedom for design.

A. Finite element simulation

The geometric nonlinearity and large displacements of the bistable MEMS problem motivated a fully nonlinear finite strain 2D elasticity model for the bistable switch which we solve using Aria.[25] Aria is a Sierra[26] framework-based parallel finite element analysis code for the solution of coupled multiphysics problems in 2D or 3D; is capable of steady-state, continuation and transient analysis; and includes support for error estimation, dynamic h-adaptivity and several nonlinear solution strategies including full Newton with analytic sensitivities (used here). In this test problem the material is taken to be a compressible neo-Hookean nonlinear elastic solid that can sustain large displacements and strains.[27] For discretization, we used standard Galerkin finite elements with either linear or quadratic quadrilateral elements with h-adaptivity and hanging node constraints.

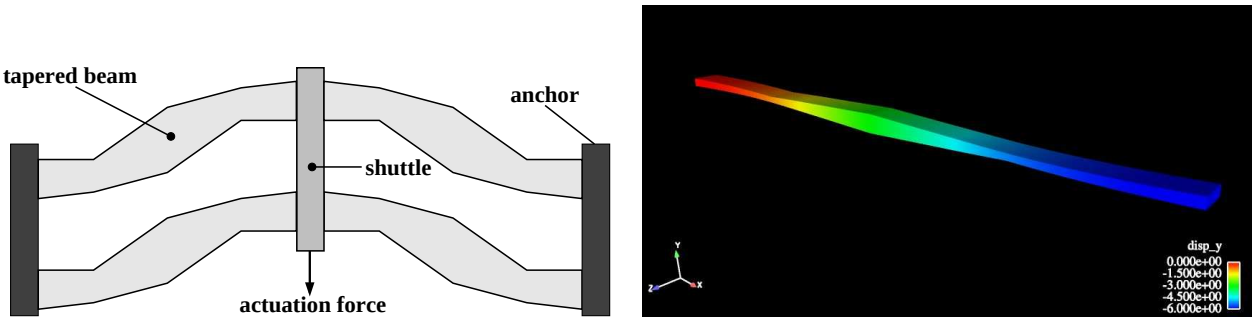

(a) Schematic of a tapered beam bistable mechanism in as-fabricated position (not to scale).

(b) Scale rendering of tapered beam leg for bistable mechanism.

Figure 2. Tapered beams for bistable MEMS mechanism.

The goal of the model is to compute the surface force response as one end of the switch is displaced, while the other end is fixed. This force is computed using the post-processed reaction force at the nodes on the specified boundary segment. For the MEMS design, the value of the force is computed throughout a range of prescribed displacements, and the minimum force is calculated by interpolation of the computed displacement-force points.

In order to compute an estimate of the error in the force at each displacement step, an *a posteriori* error estimate was derived for the force error (Section III). Formally, this "goal-oriented" estimator is defined by integrating the finite element residual weighted by the error in an associated global linearized adjoint problem. In practice, we compute a finite element approximation to the adjoint problem using the same mesh and elements as the original displacement formulation. Then the adjoint error weights are approximated as the difference between a local higher order recovered adjoint solution and the computed approximate adjoint solution.

B. Random and design variable formulation

The tapered beam legs of the bistable MEMS mechanism are parameterized by the 13 design variables shown in Figure 3, including widths and lengths of beam segments as well as angles between segments. For simulation, a symmetry boundary condition allowing only displacement in the negative y direction is applied to the right surface ($x = 0$) and a fixed displacement condition is applied to the left surface. With appropriate scaling, this allows the quarter model to reasonably represent the full four-leg switch system.

Due to manufacturing processes, fabricated geometry can deviate significantly from design-specified beam geometry. As a consequence of photo lithography and etching processes, fabricated in-plane geometry edges (contributing to widths and lengths) can be $0.1 \pm 0.08\,\mu m$ less than specified. This uncertainty in the manufactured geometry leads to substantial uncertainty in the positions of the stable equilibria and in the maximum and minimum force on the force–displacement curve. The manufactured thickness of the device is also uncertain, though this does not contribute as much to variability in the force–displacement behavior. Uncertain material properties such as Young's modulus and residual stress also influence the characteristics of the fabricated beam. For this application two key uncertain variables are considered: ΔW (edge bias on beam widths, which yields effective manufactured widths of $W_i + \Delta W, i = 0, \ldots, 4$) and S_r (residual stress in the manufactured device), with distributions shown in Table 1.

Table 1. Uncertain variables $\mathbf{x} = [\Delta W, S_r]$ used in reliability analysis.

variable	mean (μ)	std. dev.	distribution
ΔW (width bias)	-0.2 μm	0.08	normal
S_r (residual stress)	-11 Mpa	4.13	normal

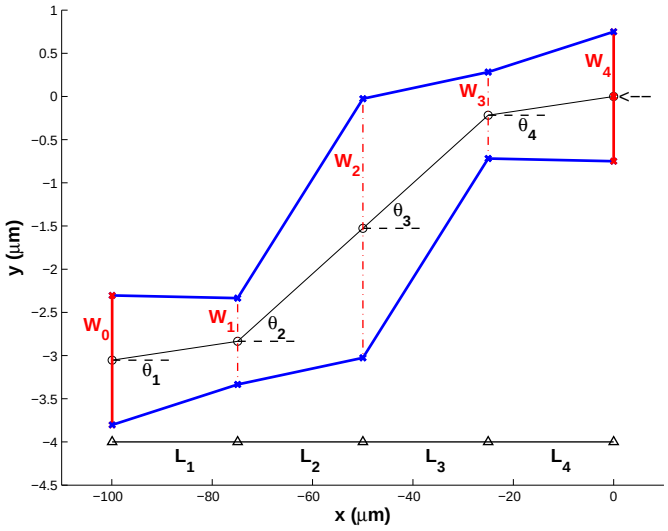

Figure 3. Design parameters for the tapered-beam fully-compliant bistable mechanism (geometry not to scale). Displacement is applied in the negative y direction at the right face ($x = 0$), while at the left face, a fixed displacement condition is enforced.

Given the 13 geometric design variables

$$\mathbf{d} = [L_1, L_2, L_3, L_4, \theta_1, \theta_2, \theta_3, \theta_4, W_0, W_1, W_2, W_3, W_4]$$

subject to the bound constraints listed in Table 3 and the specified uncertain variables $\mathbf{x} = [\Delta W, S_r]$, we formulate a reliability-based design optimization problem to achieve a design that actuates reliably with at least 5 μN force. The RBDO formulation uses the limit state

$$g(\mathbf{x}) = F_{min}(\mathbf{x}) \tag{28}$$

and failure is defined to be actuation force with magnitude less than 5.0 μN ($F_{min} > -5.0$). Reliability index $\beta_{ccdf} \geq 2$ is required. The RBDO problem utilizes the RIA $\bar{z} \rightarrow \beta$ approach (20) with $\bar{z} = -5.0$:

$$\begin{array}{lrcll} \max & & & \mathrm{E}\left[F_{min}(\mathbf{d},\mathbf{x})\right] & \\ \text{s.t.} & 2 & \leq & \beta_{ccdf}(\mathbf{d}) & \\ & 50 & \leq & \mathrm{E}\left[F_{max}(\mathbf{d},\mathbf{x})\right] & \leq \quad 150 \\ & & & \mathrm{E}\left[E_2(\mathbf{d},\mathbf{x})\right] & \leq \quad 8 \end{array} \tag{29}$$

although the PMA $\bar{\beta} \rightarrow z$ approach (21) could also be used. The use of the F_{min} metric in both the objective function and the reliability constraint results in a powerful problem formulation, because in addition to yielding a design with specified reliability, it also produces a robust design. By forcing the expected value of F_{min} toward the -5.0 target while requiring two standard deviations of surety, the optimization problem favors designs with less variability in F_{min}. This renders the design performance less sensitive to uncertainties. The response PDF control is depicted in Figure 4(a), where the mean is maximized subject to a reliability constraint on the right tail. Alternatively, the response PDF control depicted in Figure 4(b) could be employed by maximizing the PMA z level corresponding to $\bar{\beta} = -2$. This has the advantage of controlling both sides of the response PDF, but it is more computationally expensive since it requires the solution of two MPP optimization problems per design cycle instead of one. For this reason, the RIA RBDO formulation in (29) is used for all results in this section.

Throughout uncertainty analysis and design optimization using DAKOTA, for each set of specified geometric design parameters and realizations of uncertain variables, we create and mesh the tapered beam geometry and then perform finite element analysis with Aria to simulate the nonlinear elastic deformation of the beam through discrete displacement steps to produce a force–displacement curve. All switch simulations employ a quarter model (single beam), with appropriate boundary conditions and multipliers to recover the full system.

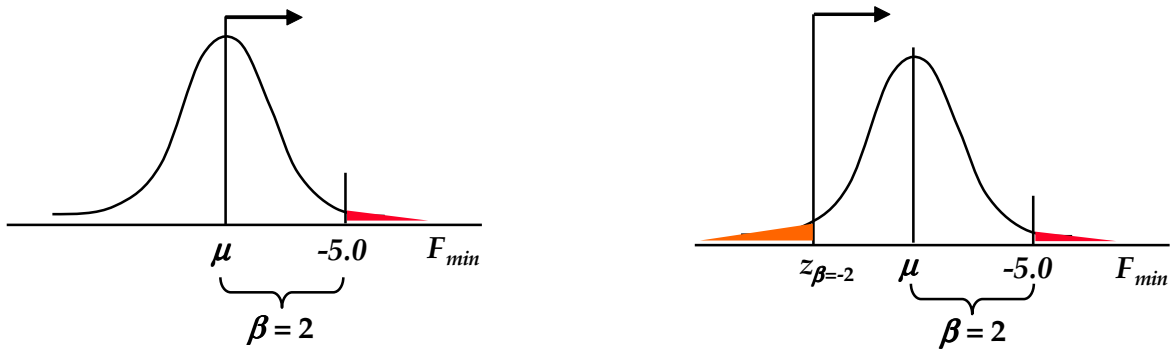

(a) Response PDF control of mean and right tail

(b) Response PDF control of both tails

Figure 4. Schematic representation of design formulations for output response PDF control.

VI. Computational Results

In this section, the reliability analysis, error estimation, and RBDO algorithms described in Sections II, III, and IV are applied to the bistable MEMS device described in Section V. Extensive computational results are reported in Ref. 28, for which the highlights are summarized here.

A. Error estimation

In Figure 5(a) we plot the force–displacement curves computed using a sequence of uniformly refined meshes of linear elements along with a fine mesh of 3200 quadratic elements, which is used as a reference solution. Looking at the entire curve, only the curves from the two coarsest meshes are clearly distinguishable from

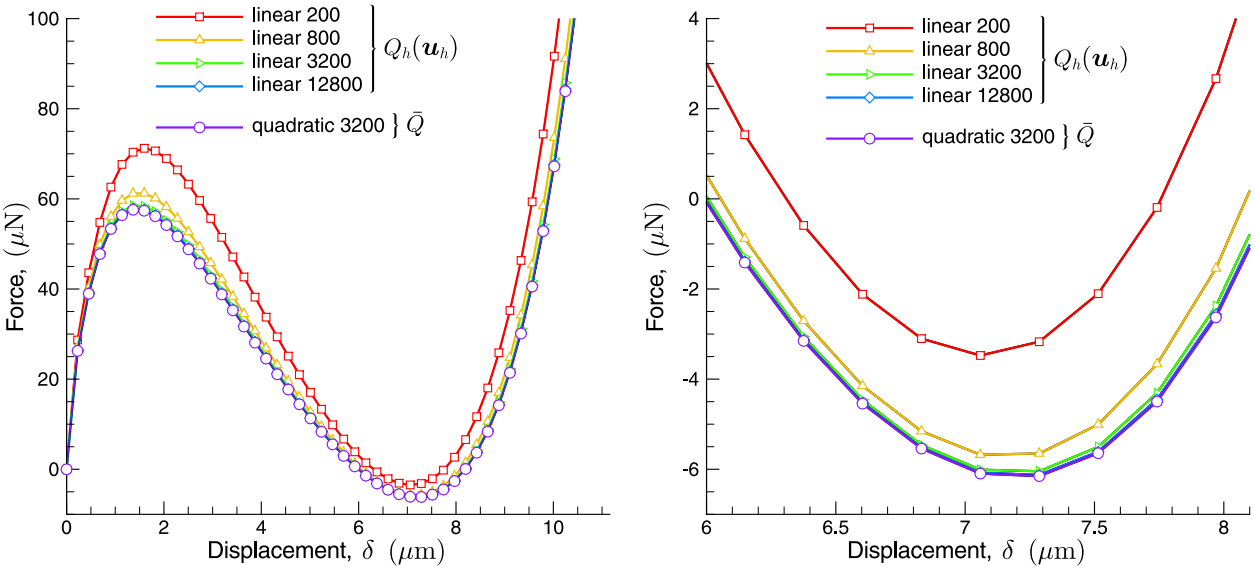

(a) Entire curve.

(b) Curve near minimum force.

Figure 5. Force–displacement curves for uniform meshes of linear elements and a fine mesh of quadratic elements.

the finer grids. However, on closer inspection in a region near the minimum force value, we see in Figure 5(b) that the rate of convergence to the reference curve is superlinear.[28]

In Figure 6(a,b) we plot the error estimator η^Q and the exact error in the surface force computed using linear elements for each displacement step. We can see that both the estimator and the exact error are typically negative, and converge to zero in absolute value as the mesh is refined. Again the error rate appears to be superlinear. In order to quantify the accuracy of η^Q, we plot in Figure 6(c) the global effectivity θ

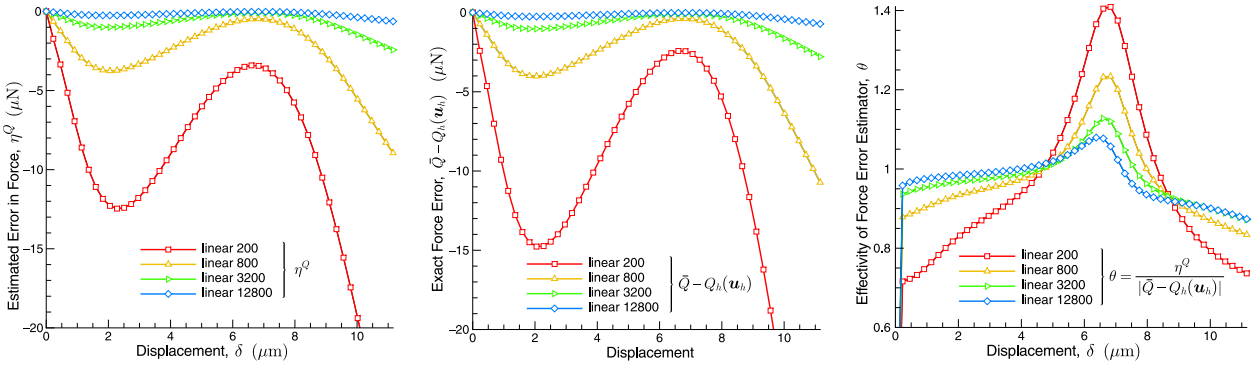

(a) Estimated error. (b) Exact error. (c) Error effectivity.

Figure 6. Estimated and exact surface force error and error effectivity for uniform meshes of linear elements.

for each displacement step. It is clear that this ratio is always between 0.7 and 1.4, and tends to one as the mesh is refined. Thus we have demonstrated that for sequences of *uniform* meshes, the estimator η^Q is a reasonable predictor of the error in the surface force for our MEMS application problem. Furthermore, the predictive capability improves as the meshes are refined.

We now turn to calculations with the error estimator η^Q in an adaptive mesh refinement algorithm. In these calculations, the nonlinear solve at each time step is wrapped in an outer adaptive iteration. The adaptive iteration proceeds through the following steps:

1. Solve the nonlinear system for u_h
2. Calculate the error estimator η^Q
3. If the error estimator exceeds the given tolerance, then apply the marking algorithm to mark elements for refinement/coarsening; otherwise exit the adaptive loop
4. Adapt the mesh based on the markers and prolongate all fields (coordinates, displacements, etc.) onto the new mesh.

We illustrate each adaptive iteration, as defined above, by plotting all of the error–displacement data points on the same graph. This means that for a given displacement step, there can be multiple output points as the adaptive algorithm adapts the mesh to minimize the global error estimator. In Figure 7(a,b), we plot such a data set for the estimated and exact error computed using the estimator η^Q and various refinement tolerances. Looking at any fixed displacement step, we can also see the number of adaptive iterations taken indicated by the points on the same vertical line. Also, we can see where the error decreases, typically from refinement of elements, and where it sometimes increases, typically from coarsening of elements. We see that while the estimator is reduced below the tolerance at each displacement step, the exact error may not be less than the tolerance. This is related to the accuracy of the estimator, which improves as the error tolerance is decreased. However, the adaptive algorithm maintains the *estimated error* to be less than the error tolerance in absolute value. The ability to adapt the mesh so that the exact error is near or below a specified tolerance is directly related to the accuracy of the error estimator. In Figure 7(c) we plot the global effectivity of the estimator η^Q. We see that even under the conditions of local mesh refinement, the error estimator is still quite accurate throughout the series of displacement steps.

B. Reliability analysis

Figure 8 shows results for reliability analysis of the MEMS bistable mechanism. Cumulative distribution functions (CDFs) are used to display the results from PMA-based reliability analyses. In Figure 8(a),

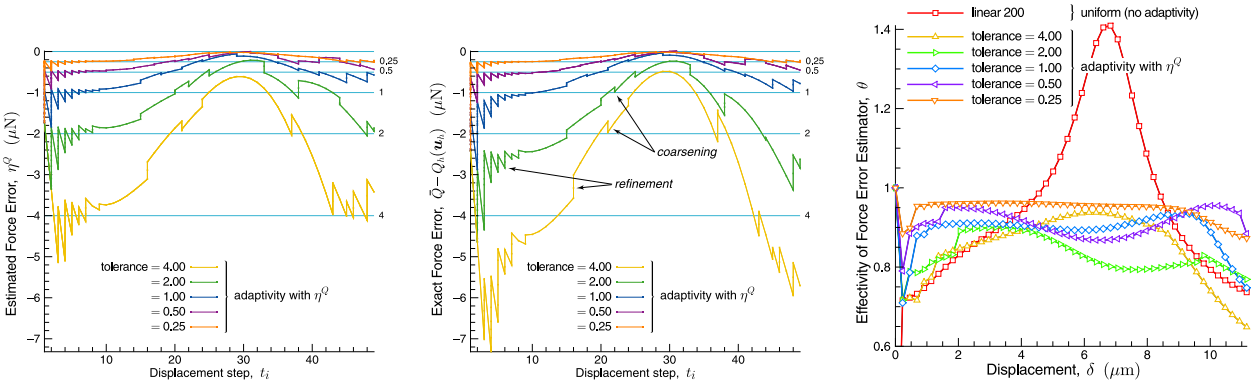

(a) Estimated error. (b) Exact error. (c) Error effectivity.

Figure 7. Estimated and exact surface force error and error effectivity for adaptive meshes using η^Q for all iterations.

convergence of the CDFs is shown for a sequence of meshes using linear elements (200, 800, 3200, and 12800 elements), and in Figure 8(b), error-corrected results are presented for the two coarsest meshes. It is evident that very nearly the same results are obtained for the reference mesh (3200 quadratic elements) and the 800 linear element mesh including error corrections.

Table 2 shows the computational time required for each of these analyses in terms of both function evaluations and average time per evaluation as well as the discrete L^2 error in minimum force values between the various approximations and the reference CDF, calculated over the 13 requested probability levels $\bar{p}_i$. The L^2 error for the finest linear mesh considered (12800 elements) is 3.1199e-02 μN, with Aria evaluations requiring, on average, 388 seconds. Using the error correction on a linear mesh with only 800 elements yields an error of 7.6341e-02 μN, with evaluations averaging 35 seconds, less than 10% of the cost. The linear elements converge at approximately second order, while the error-corrected linear elements and quadratic elements converge at approximately fourth order.[28] Since the inclusion of adjoint error estimation calcula-

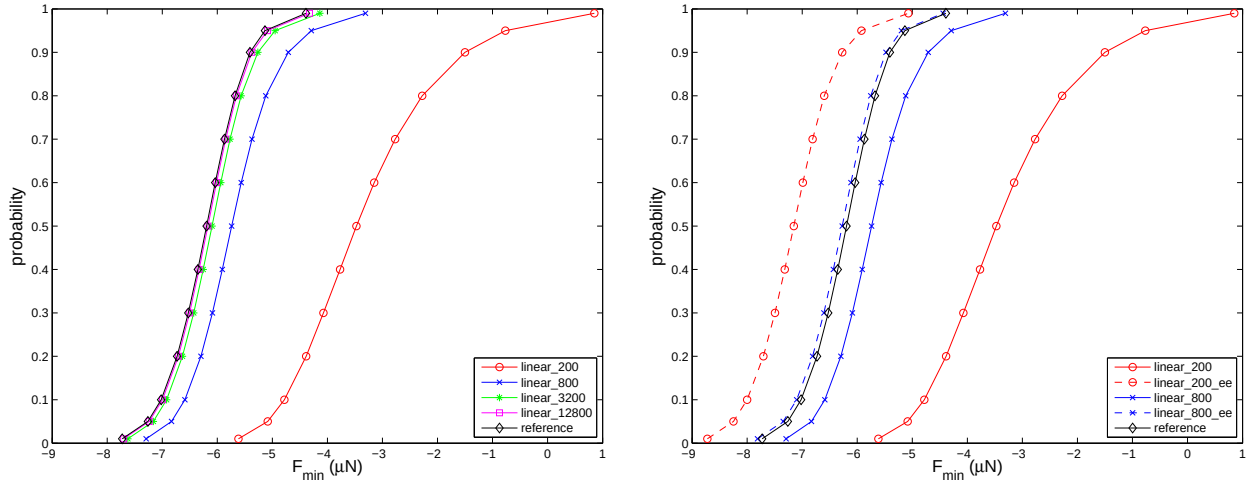

(a) CDF convergence without error correction (b) CDF convergence with error correction

Figure 8. Cumulative distribution functions for F_{min} for a set of uniformly-refined meshes with and without error correction.

tions only adds 46–49% to the nominal per-simulation cost, a quantitatively-predictive error correction on a coarse mesh can significantly outperform a fully-converged fine mesh (which can be orders of magnitude

more expensive). However, the error estimates are not always quantitatively predictive, and it is evident from the 200 linear element results in Figure 8 that a level of mesh convergence is still required for the error estimates to be predictive, however the level of mesh convergence required with error estimates is much lower than without. This points to the use of a combination of error control and error correction, where mesh adaptivity is first used to obtain a mesh where the estimator can be quantitatively predictive (but the mesh is not refined to the point of driving the error to zero), and then the estimate is applied as a correction factor. Refer to Ref. 28 for additional information on these combined approaches.

Table 2. Computational cost and error for 13 point CDF generated with various meshes.

FEA type	UQ method	num. elts.	num. nodes	func. evals	time per eval (sec)	L^2 error in $z = F_{min}$
linear	AMV^2+	200	303	340	5.7767	3.1758e+00
linear w/EE	AMV^2+	200	303	485	8.5953	9.2555e-01
linear	AMV^2+	800	1005	410	23.4885	5.8753e-01
linear w/EE	AMV^2+	800	1005	445	34.6055	7.6341e-02
linear	AMV^2+	3200	3609	475	93.2751	1.2985e-01
linear w/EE	AMV^2+	3200	3609	420	136.2651	6.0263e-03
linear	AMV^2+	12800	13617	425	388.3487	3.1199e-02
linear w/EE	AMV^2+	12800	13617	470	568.3060	7.0266e-04
quadratic	AMV^2+	3200	13617	360	477.8220	

C. RBDO

The RBDO problem is solved by applying the DAKOTA software in the bi-level (nested) approach of Section IV using semi-analytic derivatives of reliability metrics with respect to design variables for the optimizer. Design variable optimization is performed with the DOT optimizer using the modified method of feasible directions (MMFD)[29] and each RIA reliability analysis is performed using AMV^2+ approximations with SR1 quasi-Hessians to solve the MPP optimization subproblems. The initial iterate for the gradient-based MMFD is taken to be an optimal design point from Ref. 2, which is already in the vicinity of the desired solution. Optimization is performed for various discretizations and error corrections, each starting from this initial iterate.

Table 3 contains optimal RBDO designs corresponding to the coarse (800 element) linear mesh, with and without η^Q error correction, the finest (12800 element) linear mesh, and the reference quadratic mesh. In all except the reference mesh case, the optimizer progresses to an optimal solution where the reliability constraint β is active and the expected value of F_{min} is maximized. The optimizer progresses when using the reference mesh, but does not yield as good a value for F_{min}, nor as tight a constraint on the reliability metric β. For all meshes considered, reliability-based design optimization finds device designs more robust to input uncertainties by the means depicted in Figure 4(a). The initial bistable MEMS design reported in Ref. 2 had variability in F_{min} of 5.6 μN per input standard deviation, calculated as $\frac{\mathrm{E}[F_{min}]-\bar{F}_{min}}{\beta}$. As shown in Table 3, the optimal designs found with the present methods have variability 0.59–0.62 μN per input standard deviation, indicating less sensitivity to input uncertainties. The error-corrected 800 element coarse mesh yields a similar solution to the 12800 element fine mesh, but at less than 10% of the total computational cost (27 versus 373 compute hours).

Figure 9 shows curves generated using the reference mesh for each of the optimal design parameter sets from Table 3. These "reference-verified" force-displacement curves further confirm that RBDO using the 800 linear element mesh, with η^Q error-correction, yields an optimal design similar to the finest (12800 element) mesh at much lower cost. Without error correction, however, the 800 linear element results have considerable discrepancy.

Table 3. RBDO results for MEMS bistable mechanism: optimal designs using AMV^2+ for four meshes.

variable or metric			initial	optimal			
			quadratic	linear	linear	linear	quadratic
l.b.	name	u.b.	3200	800	800 w/EE	12800	3200
10	$L_1\,(\mu m)$	35	28.06	28.33	28.07	28.04	28.08
10	$L_2\,(\mu m)$	35	24.50	24.61	24.44	24.42	24.47
10	$L_3\,(\mu m)$	35	30.83	31.05	30.63	30.59	30.72
10	$L_4\,(\mu m)$	35	30.83	31.08	30.61	30.56	30.70
0	θ_1 (deg.)	5	4.167	4.170	4.195	4.198	4.184
0	θ_2 (deg.)	5	2.500	2.514	2.485	2.482	2.491
0	θ_3 (deg.)	5	2.500	2.523	2.472	2.467	2.484
0	θ_4 (deg.)	5	2.400	2.410	2.387	2.385	2.393
1	$W_0\,(\mu m)$	3	1.333	1.313	1.349	1.354	1.342
1	$W_1\,(\mu m)$	3	1.253	1.233	1.268	1.273	1.260
2	$W_2\,(\mu m)$	5	3.500	3.505	3.485	3.482	3.491
1	$W_3\,(\mu m)$	3	2.000	1.993	2.005	2.006	2.004
1	$W_4\,(\mu m)$	3	1.333	1.327	1.334	1.333	1.334
	$\mathrm{E}\,[F_{min}]\;(\mu N)$		-6.645	-6.208	-6.231	-6.188	-6.288
2	β		2.172	1.998	1.998	2.002	2.094
50	$\mathrm{E}\,[F_{max}]\;(\mu N)$	150	57.05	59.19	57.65	57.87	57.11
	$\mathrm{E}\,[E_2]\;(\mu m)$	8	6.019	6.156	6.002	5.996	6.021
var. in F_{min} per β			0.76	0.60	0.62	0.59	0.62
num. func. evals.			-	3581	2822	3149	1750
avg. time/eval (sec)			-	24.0552	34.4634	425.8951	479.9207

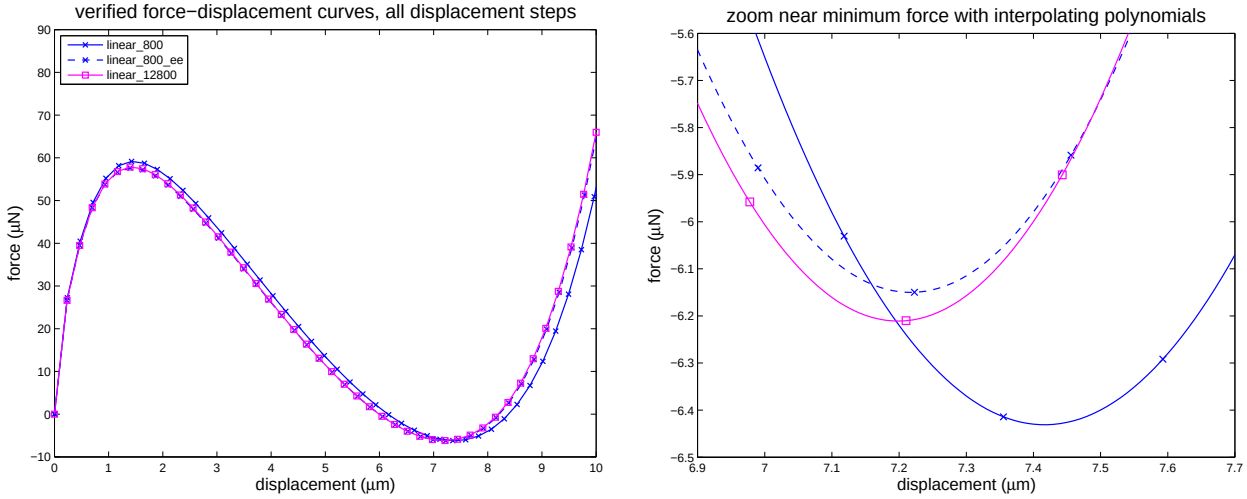

(a) Entire curve.

(b) Curve near minimum force.

Figure 9. Verified force–displacement curves generated using reference mesh (3200 quadratic elements) with optimal geometries defined from RBDO on various meshes.

VII. Conclusions

This paper explores the benefits of embedding automated solution verification within uncertainty analyis for the probabilistic analysis and design of microelectromechanical systems (MEMS). An error estimator is

developed for the error in the surface force in finite element approximations of nonlinear elasticity models. Numerical results verify that the estimator produces accurate error estimates using both uniform and adaptively-refined meshes. Error-corrected and error-controlled reliability analysis using the estimator are applied to address solution verification in an automated, on-line manner. Any dependence of solution discretization errors on random or design variables, which can occur particularly when varying geometric shape parameters, is captured. The most effective and affordable of these approaches are carried forward in probabilistic design studies for robust and reliable operation of a bistable MEMS device.

The key paper conclusion is that on-line solution verification approaches show significant promise. In terms of accuracy, controlling or correcting for errors (or both) leads to higher confidence in the uncertainty analysis and probabilistic design recommendations. In terms of computational expense, the use of error-correction on coarse meshes (from adjoint-based quantity of interest error estimates) was shown to result in less than 10% of the simulation expense of fully converged meshes with comparable accuracy. In terms of computational reliability, the ability of the on-line approach to be parameter-adaptive precludes the possibility of using model results that are converged for one set of parameters, but not for another. And in terms of convenience, the potential elimination of the need for manual convergence studies should significantly reduce overhead for analysts and designers.

Table 4 summarizes these characteristics for different approaches to solution verification within UQ/RBDO studies, including no solution verification, off-line solution verification at the simulation level (e.g., Figure 5(a)), off-line solution verification at the UQ/RBDO study level (e.g., Figure 8(a)), and on-line solution verification using error estimation and adaptivity. Of these possibilities, the no verification and simulation-level off-line approaches are believed to be the two most common practices at this time. The on-line approaches are clearly the most desirable, but are obtained at the price of additional simulation development to support error estimation and adaptivity.

	no verification	simulation-level off-line	study-level off-line	on-line EE/Adapt
Accuracy	L	M	H	H
Efficiency	H	M	L	H
Reliability	L	M	H	H
Convenience	H	M	L	H

Table 4. Comparison of solution verification strategies: H = high, M = medium, L = low

Acknowledgments

The authors thank David Neckels and Sam Subia for their assistance in developing error estimation capabilities within Aria, and Barron Bichon for assistance in investigating reliability method performance.

References

[1]Allen, J. J., *Micro Electro Mechanical System Design*, Taylor and Francis, Boca Raton, 2005.

[2]Adams, B. M., Eldred, M. S., and Wittwer, J. W., "Reliability-Based Design Optimization for Shape Design of Compliant Micro-Electro-Mechanical Systems," *Proceedings of the 11th AIAA/ISSMO Multidisciplinary Analysis and Optimization Conference*, No. AIAA-2006-7000, Portsmouth, VA, September 6–8, 2006.

[3]Eldred, M. S., Agarwal, H., Perez, V. M., Wojtkiewicz, Jr., S. F., and Renaud, J. E., "Investigation of Reliability Method Formulations in DAKOTA/UQ," *Structure & Infrastructure Engineering: Maintenance, Management, Life-Cycle Design & Performance*, to appear.

[4]Eldred, M. S. and Bichon, B. J., "Second-Order Reliability Formulations in DAKOTA/UQ," *Proceedings of the 47th AIAA/ASME/ASCE/AHS/ASC Structures, Structural Dynamics and Materials Conference*, No. AIAA-2006-1828, Newport, RI, May 1–4 2006.

[5]Rosenblatt, M., "Remarks on a Multivariate Transformation," *Ann. Math. Stat.*, Vol. 23, No. 3, 1952, pp. 470–472.

[6]Der Kiureghian, A. and Liu, P. L., "Structural Reliability Under Incomplete Probability Information," *J. Eng. Mech., ASCE*, Vol. 112, No. 1, 1986, pp. 85–104.

[7]Box, G. E. P. and Cox, D. R., "An Analysis of Transformations," *J. Royal Stat. Soc.*, Vol. 26, 1964, pp. 211–252.

[8]Rackwitz, R. and Fiessler, B., "Structural Reliability under Combined Random Load Sequences," *Comput. Struct.*, Vol. 9, 1978, pp. 489–494.

[9]Chen, X. and Lind, N. C., "Fast Probability Integration by Three-Parameter Normal Tail Approximation," *Struct. Saf.*, Vol. 1, 1983, pp. 269–276.

[10]Wu, Y.-T. and Wirsching, P. H., "A New Algorithm for Structural Reliability Estimation," *J. Eng. Mech., ASCE*, Vol. 113, 1987, pp. 1319–1336.

[11]Tu, J., Choi, K. K., and Park, Y. H., "A New Study on Reliability-Based Design Optimization," *J. Mech. Design*, Vol. 121, 1999, pp. 557–564.

[12]Eldred, M. S., Brown, S. L., Adams, B. M., Dunlavy, D. M., Gay, D. M., Swiler, L. P., Giunta, A. A., H art, W. E., Watson, J.-P., Eddy, J. P., Griffin, J. D., Hough, P. D., Kolda, T. G., Martinez-Canales, M. L., and Williams, P. . J., "DAKOTA, A Multilevel Parallel Object-Oriented Framework for Design Optimization, Parameter Estimation, Uncertainty Quantification, and Sensitivity Analysis: Version 4.0 Users Manual," Tech. Rep. SAND2006-6337, Sandia National Laboratories, Albuquerque, NM, 2006.

[13]Allen, M. and Maute, K., "Reliability-based Design Optimization of Aeroelastic Structures," *Struct. Multidiscip. O.*, Vol. 27, 2004, pp. 228–242.

[14]Wu, Y.-T., Shin, Y., Sues, R., and Cesare, M., "Safety-Factor Based Approach for Probability-Based Design Optimization," *Proceedings of the 42rd AIAA/ASME/ASCE/AHS/ASC Structures, Structural Dynamics, and Materials Conference*, No. AIAA-2001-1522, Seattle, WA, April 16–19, 2001.

[15]Du, X. and Chen, W., "Sequential Optimization and Reliability Assessment Method for Efficient Probabilistic Design," *J. Mech. Design*, Vol. 126, 2004, pp. 225–233.

[16]Agarwal, H., Renaud, J. E., Lee, J. C., and Watson, L. T., "A Unilevel Method for Reliability Based Design Optimization," *Proceedings of the 45th AIAA/ASME/ASCE/AHS/ASC Structures, Structural Dynamics, and Materials Conference*, No. AIAA-2004-2029, Palm Springs, CA, April 19–22, 2004.

[17]Hohenbichler, M. and Rackwitz, R., "Sensitivity and Importance Measures in Structural Reliability," *Civil Eng. Syst.*, Vol. 3, 1986, pp. 203–209.

[18]Karamchandani, A. and Cornell, C. A., "Sensitivity Estimation within First and Second Order Reliability Methods," *Struct. Saf.*, Vol. 11, 1992, pp. 95–107.

[19]Kemeny, D. C., Howell, L. L., and Magleby, S. P., "Using Compliant Mechanisms to Improve Manufacturability in MEMS," *Proc. 2002 ASME DETC*, No. DETC2002/DFM-34178, 2002.

[20]Ananthasuresh, G. K., Kota, S., and Gianchandani, Y., "A Methodical Approach to the Design of Compliant Micromechanisms," *Proc. IEEE Solid-State Sensor and Actuator Workshop*, Hilton Head Island, SC, 1994, pp. 189–192.

[21]Jensen, B. D., Parkinson, M. B., Kurabayashi, K., Howell, L. L., and Baker, M. S., "Design Optimization of a Fully-Compliant Bistable Micro-Mechanism," *Proc. 2001 ASME Intl. Mech. Eng. Congress and Exposition*, New York, NY, November 11–16, 2001.

[22]Wittwer, J. W., *Simulation-based Design under Uncertainty for Compliant Microelectromechanical Systems*, Ph.D. thesis, Brigham Young University, Salt Lake City, UT, April 2005.

[23]Wittwer, J. W., Baker, M. S., and Howell, L. L., "Robust Design and Model Validation of Nonlinear Compliant Micromechanisms," *J. Microelectromechanical Sys.*, Vol. 15, No. 1, 2006, to appear.

[24]Qiu, J. and Slocum, A. H., "A Curved-beam Bistable Mechanism," *J. Microelectromech. Syst.*, Vol. 13, No. 2, 2004, pp. 137–146.

[25]Notz, P. K., Subia, S. R., Hopkins, M. H., and Sackinger, P. A., "A Novel Approach to Solving Highly Coupled Equations in a Dynamic, Extensible and Efficient Way," *Computation Methods for Coupled Problems in Science and Engineering*, edited by M. Papadrakakis, E. . Onate, and B. Schrefler, Intl. Center for Num. Meth. in Engng. (CIMNE), Barcelona, Spain, April 2005, p. 129.

[26]Edwards, H. C., "Sierra Framework for Massively Parallel Adaptive Multiphysics Application," Tech. Rep. SAND2004-6277C, Sandia National Laboratories, Albuquerque, NM, July 2005.

[27]Bonet, J. and Wood, R. D., *Nonlinear continuum mechanics for finite element analysis*, Cambridge University Press, 1997.

[28]Adams, B. M., Bichon, B. J., Eldred, M. S., Carnes, B., Copps, K. D., Neckels, D. C., Hopkins, M. M., Notz, P. K., Subia, S. R., and Wittwer, J. W., "Solution-Verified Reliability Analysis and Design of Bistable MEMS Using Error Estimation and Adaptivity," Tech. Rep. SAND2006-6286, Sandia National Laboratories, Albuquerque, NM, 2006.

[29]Vanderplaats Research and Development, Inc., Colorado Springs, CO, *DOT Users Manual, Version 4.20*, 1995.